UW-CPTC--97-21

UNIVERSITY OF WISCONSIN

CENTER FOR PLASMA THEORY AND COMPUTATION

REPORT

Tearing mode analysis in tokamaks, revisited

Y. Nishimura, J. D. Callen, and C. C. Hegna

Department of Engineering Physics
University of Wisconsin-Madison
Madison, Wisconsin 53706-1687

December 1997

UW-CPTC 97-21

MADISON, WISCONSIN 53706-1687

Tearing mode analysis in tokamaks, revisited

Y. Nishimura, J. D. Callen, and C. C. Hegna

Department of Engineering Physics

University of Wisconsin-Madison, Wisconsin, 53706-1687

Abstract

A new Δ' shooting code has been developed to investigate tokamak plasma tearing mode stability in a cylinder and large aspect ratio ($\epsilon \leq 0.25$) toroidal geometries, neglecting toroidal mode coupling. A different computational algorithm is used (shooting out from the singular surface instead of into it) to resolve the strong singularities at the mode rational surface, particularly in the presence of finite pressure term. Numerical results compare favorably with Furth et al. [H. P. Furth et al., Phys. Fluids **16**, 1054 (1973)] results. The effects of finite pressure, which are shown to decrease Δ', are discussed. It is shown that the distortion of the flux surfaces by the Shafranov shift, which modifies the geometry metric elements stabilizes the tearing mode significantly, even in a low β regime before the toroidal magnetic curvature effects come into play. Double tearing modes in toroidal geometries are examined as well. Furthermore, $m \geq 2$ tearing mode stability criteria are compared with three dimensional initial value MHD simulation by the FAR code [L. A. Charlton et al., J. Comp. Phys. **63**, 107 (1986)].

PACS numbers: 52.30.Jb, 52.35Py, 52.55.Fa, 52.65

I. INTRODUCTION

Understanding resistive magnetohydrodynamic (MHD) stability is important for long pulse tokamak operations, since tearing modes form magnetic islands, and if islands of incommensurate helicity overlap, they can induce plasma disruptions.[1] Also, the existence of a single helicity magnetic island can deteriorate plasma confinement due to the change in magnetic field line topology.[2,3] In resistive MHD, tearing mode stability is determined by a parameter delta prime (Δ'), which was first defined by Furth et al.;[4] a positive Δ' implies instability. Recently, Δ' was measured in Tokamak Test Fusion Reactor (TFTR) supershot plasma experiments through an analysis of electron temperature fluctuations.[5] It has been shown that when $m/n = 2/1$ modes are present, $\Delta' > 0$. This can be explained by classical tearing mode theory. On the other hand, Δ' is observed to be negative for cases with $m/n = 3/2$ and $m/n = 4/3$ modes, which indicates the presence of destabilizing neoclassical effects.[6] The qualitative framework of tearing mode theory seems to be well established.

In toroidal tokamak plasmas, Fourier harmonics of tearing modes are correlated to each other, both through the poloidal mode coupling and nonlinear effects. These couplings can play an important role in destabilizing the modes on magnetic surfaces of incommensurate helicity. The final goal of our research is to investigate such a multi-mode coupled system, for example, as pursued in the PEST-3 code.[7] However, quantitative determination of the tearing mode stability parameter Δ' still remains an essential issue: a precise prediction of stability becomes important, especially when the tearing modes are marginally stable ($|\Delta'| \lesssim 0$). The value of Δ' is sensitive to the local current gradient even in the single helicity case. For the purpose of seeking optimized discharge current profiles for the experiments and simultaneous feedback control,[8] it is important to understand and clarify the nature of the numerical procedures that correctly relate Δ' to the current profile.

A shooting-type code[9] for determining the perturbed helical flux profile and hence Δ' is compact, intuitively straightforward, and has fast convergence. Obtaining a Δ' value for a single helicity case takes less than a second of cpu-time on nominal workstation computers.

This fast convergence is tractable for developing a feedback stabilization scheme for controlling tearing modes in tokamak discharges.[8]

Finite pressure effects were ignored in the previous analyses by Furth et al.[9] and Wesson.[10] This is due to the fractional power-like singularity that arises at the mode rational surface when pressure gradient effects are present. Furthermore, difficulties arise in separating the large and the small solutions near the rational surface.[11] In this work, a different type of numerical algorithm was employed (integrate out from the singular surface rather than into it). The algorithm converges correctly in a high β ($\beta \geq 7\%$) regime for cylindrical geometry (β represents the ratio between the plasma and magnetic pressure). To check the validity of our computational results, we start (see Section III) by comparing our results with the Furth et al.[9] results for zero-pressure cases.

The effects of toroidal geometry are considered in this work. The effects can be separated into (1) distortion of the flux surfaces due to the Shafranov shift; (2) the existence of an averaged magnetic well; and (3) mode coupling effects due to the $1/R$ dependence of the magnetic field which is neglected here. We have included (1) and (2), and obtained Δ' as a function of β.[12] The Shafranov shift appear as a global effect contribution that enters through changes in the geometry metric elements. The second effect appears as a localized property near the mode rational surface; we have included toroidal curvature (the Mercier index[13]) in the analysis, but have not included resistive layer effects.[14] The mode coupling effect can be neglected in the case of a rotating tokamak plasma where shear flows are large and modes at different surfaces decouple.[15]

As an example of multi-helicity mode analysis by the shooting method, we present initial results for double tearing modes that are considered as a cause of an off axis sawtooth in the recent experiments of reversed shear discharge in TFTR.[16] The growth rate predicted by Δ' is compared with that obtained from the toroidal magnetohydrodynamic initial value code FAR.[17]

This paper is organized as follows. In Sec. II the original definition and the physical significance of Δ' is discussed. In Sec. III the basic model of Furth et al.[9] for the exterior

region is presented and our Δ' calculation is compared with their results. The logarithmic singularity at the resistive layer as well as the algorithm for solving the boundary value problem are discussed in detail. Finite pressure effects are discussed in Sec. IV. The effects of toroidal geometry are introduced in Sec. V. Double tearing modes in toroidal geometry are discussed in Sec. VI. Finally, we summarize in Sec. VII.

II. THE DEFINITION OF Δ'

The physical significance of the sign of Δ' can be understood intuitively from the one dimensional magnetic field line diffusion equation given by Faraday's law and the Ohm's law:[18]

$$\frac{\partial \tilde{B}_r}{\partial t} = \frac{\eta}{\mu_0}\nabla^2 \tilde{B}_r \sim \frac{\eta}{\mu_0}\frac{\partial^2 \tilde{B}_r}{\partial r^2}, \tag{1}$$

where η and μ_0 stand for the plasma resistivity and vacuum magnetic permeability respectively. According to Ref. 18, it can be seen that if $\partial^2 \tilde{B}_r/\partial r^2 < 0$ then $\partial \tilde{B}_r/\partial t < 0$ and perturbation damps in the initial phase. On the other hand, if $\partial^2 \tilde{B}_r/\partial r^2 > 0$ then $\partial \tilde{B}_r/\partial t > 0$ and perturbation grows.

The plasma column is divided into two "exterior regions"[4] by a resistive layer of width δ. The mode rational surface where $q = m/n$ resides in this thin layer. Eigenmode profiles are connected from one exterior region to the other via resistive layer properties. Thus, there is a jump discontinuities in the slope between the two exterior regions. If the eigenfunction is locally convex (concave), the mode is stable (unstable). Furth et al.[4] defined Δ' as the difference of the slopes for the flux function ψ inside and outside the mode rational surface x_s:

$$\Delta' \equiv \frac{\psi'_+(x_s+\delta) - \psi'_-(x_s-\delta)}{\psi(x_s)}, \tag{2}$$

where a positive Δ' implies instability. Note that the Δ' value indicates the relative jump in $\tilde{B}_r$ across the inner layer, and hence to a current sheet in the inner layer.

III. REVIEW OF CYLINDRICAL FORMULATION AND COMPUTATION

In this section, the basic model equation (the exterior equation) and the results of Ref. 9 are reviewed. A cylindrical coordinate system is employed in the calculation, where r is the minor radius, θ is the poloidal angle, and z is in the toroidal direction. Combining the momentum balance equation, Faraday's law, Ohm's law, and plasma incompressibility in a cylindrical geometry, we obtain the Newcomb equation[9,19]

$$\frac{d^2\psi}{dr^2} + \frac{1}{H}\frac{dH}{dr}\frac{d\psi}{dr} - \frac{1}{H}\left[\frac{g}{F^2} + \frac{1}{F}\frac{d}{dr}\left(H\frac{dF}{dr}\right)\right]\psi = 0, \tag{3}$$

where

$$F \equiv \mathbf{k}\cdot\mathbf{B} = kB_z + (m/r)\,B_\theta = \frac{B_z}{R}\,(1 - m/q)\,,$$
$$H \equiv \frac{r^3}{k^2r^2 + m^2},$$
$$g \equiv \frac{(m^2-1)rF^2}{k^2r^2+m^2} + \frac{k^2r^2}{k^2r^2+m^2}\left[rF^2 + F\frac{2(krB_z - mB_\theta)}{k^2r^2+m^2} + \frac{dP}{dr}\right].$$

Note that the toroidal mode number is taken to be $n = 1$ throughout this paper. After normalization using $x \equiv r/r_s$ (r_s is the mode rational surface radius), $b \equiv B_\theta/B_z$, and $p \equiv (P/\beta)2B_z^2$ ($\beta \equiv P_0/2\mu_0 B_z^2$ is a figure of merit that represents the ratio between the plasma and magnetic pressure), Eq. (3) reduces to

$$\psi'' + g_2(x)\,\psi' - g_1(x)\,\psi = 0, \tag{4}$$

where we have further defined

$$g_1(x) \equiv \frac{1}{H}\left[\frac{g}{F^2} + \frac{1}{F}\left(HF'\right)'\right],$$
$$g_2(x) \equiv \frac{H'}{H}.$$

In Eq. (4), the prime denotes differentiation with respect to x. Here, the poloidal magnetic field profile, and safety factor are taken to be the peaked profile of Ref. 9:

$$b(x) = \frac{x}{(1+x^2)}, \tag{5}$$

$$q(x) = q_0\left(1 + x^2\right). \tag{6}$$

The plasma boundary is located at $x_b = 2$ while the mode rational surface is varied by changing the q_0 value. The pressure profile was taken to be $p = 0$ for the zero β case and $p(x) = 1 - (x/x_b)^2$ for the finite β case which we discuss in Sec. V.

The numerical algorithm of the shooting method will now be explained. In the vicinity of the rational surface and in the absence of plasma pressure ($\beta = 0$), Eq. (4) reduces to the form

$$\frac{d^2\psi}{d^2\mathcal{X}} - \frac{\kappa}{\mathcal{X}}\psi = 0 \tag{7}$$

where $\mathcal{X} = x - x_s$ and $\kappa = g_1(x_s)$. The inner limit of the exterior asymptotic solutions

$$\psi = \left(1 + \kappa\mathcal{X}\ln|\mathcal{X}| + \frac{1}{2}\kappa^2\mathcal{X}^2\ln|\mathcal{X}| - \frac{3}{4}\kappa^2\mathcal{X}^2 + ...\right) + A_{I,III}\left(\mathcal{X} + \frac{1}{2}\kappa\mathcal{X}^2 + \frac{1}{12}\kappa^2\mathcal{X}^3 + ...\right) \tag{8}$$

are matched to the numerical solutions at $\mathcal{X} = \pm\delta$. Here, the subscripts 'I' and 'III' denote the two exterior regions inside and outside the mode rational surface x_s. We solve Eq. (4) by numerically *shooting* away from the singular surface with an arbitrary boundary condition toward the other ends at $x = 0$ and $x = x_b$, and iterate until the boundary conditions there are satisfied. (This is in the opposite way from Furth et al.,[9] where the shooting was done from the boundaries inward and numerical solutions near x_s were fit to the asymptotic solution). We solve Eq. (4) in the two regions $0 \le x \le x_s$ and $x_s \le x \le x_b$ obtaining ψ_I and ψ_{III}. Defining $\mathbf{Y} = (y_1, y_2, y_3, y_4) = (\psi, \psi', \partial\psi/\partial A_{I,III}, \partial\psi'/\partial A_{I,III})$, Eq. (4) reduces to a system of simultaneous ordinary differential equations

$$\frac{d\mathbf{Y}}{dx} = \begin{pmatrix} y_1' \\ y_2' \\ y_3' \\ y_4' \end{pmatrix} = \begin{pmatrix} y_2 \\ -g_2(x)y_2 + g_1(x)y_1 \\ y_4 \\ -g_2(x)y_2 + g_1(x)y_1 \end{pmatrix}, \tag{9}$$

with boundary conditions at $x = x_s \pm \delta$:

$$\begin{pmatrix} y_1 \\ y_2 \\ y_3 \\ y_4 \end{pmatrix} = \begin{pmatrix} \left(1+\kappa\delta\ln|\delta|+\frac{1}{2}\kappa^2\delta^2\ln|\delta|-\frac{3}{4}\kappa^2\delta^2\right)+A_{I,III}\left(\delta+\frac{1}{2}\kappa\delta^2+\frac{1}{12}\kappa^2\delta^3\right) \\ \kappa(\ln\delta+1)+\kappa^2\left(\delta\ln|\delta|-\delta\right)+A_{I,III}\left(1+\kappa\delta+\frac{1}{4}\kappa^2\delta^2\right) \\ \delta+\frac{1}{2}\kappa\delta^2+\frac{1}{12}\kappa^2\delta^3 \\ 1+\kappa\delta+\frac{1}{4}\kappa^2\delta^2 \end{pmatrix}. \tag{10}$$

A fourth order Runge-Kutta-Gill method[20] is used for the numerical integration. One changes the unknown constant $A_{I,III}$ until the values $A^{l+1}-A^l=-(\psi)/(\partial\psi/\partial A)$ at the boundaries converge (l represents the iteration step). The value of Δ' is calculated by

$$\Delta' = \frac{\psi'_{III}(x_s+\delta)-\psi'_I(x_s-\delta)}{\psi(x_s)} = A_{III}-A_I. \tag{11}$$

For a comparison with Furth et al.,[9] we take the poloidal/toroidal mode numbers to be $m/n = 2/1$, while a large aspect ratio is represented by $kr_0 = 0.05$. Figure 1(a) shows the eigenmode profile while Fig. 1(b) shows the value of Δ' as a function of mode rational surfaces x_s. Figure 1(b) implies that the tearing modes are relatively stable when the mode rational surfaces are closer to the plasma boundary. The results match exactly with Fig.1 of Ref. 9. (Note that the numerical algorithm we employed is quite different). We have also reproduced the numerical results by Wesson[10] (see the Appendix A).

IV. EIGENMODE SOLUTIONS IN THE PRESENCE OF FINITE PRESSURE

An algorithm for cases with the pressure term is discussed in this section. In the presence of finite pressure effects, the exterior equation Eq.(4) has strong singularities with two independent solutions called large (dominant) and the small (subdominant),[11] exhibiting different fractional power-like asymptotic behaviors:

$$\psi = A_I|\mathcal{X}|^{h+1} - B_I|\mathcal{X}|^{-h}, \tag{12}$$

in region I, and

$$\psi = A_{III}|\mathcal{X}|^{h+1} + B_{III}|\mathcal{X}|^{-h}, \tag{13}$$

in region III. Here $h = -\frac{1}{2} + \frac{1}{2}\sqrt{1-4D_s}$, $D_s \equiv \beta\left(-2q^2/{q'}^2{B_z}^2 x\right)(dp/dx)\,|_{x=x_s}$,[11] and $\mathcal{X} = x - x_s$ as before. Note that in the $h = 0$ limit, this reduces to the same form as the zero-pressure case. As in the $\beta = 0$ case, the asymptotic solutions Eqs. (12) and (13) at the resonant surface are matched to the numerical solution.

Defining $\mathbf{Y} = (y_1, y_2, y_3, y_4, y_5, y_6) = \left(\psi, \psi', \partial\psi/\partial A, \partial\psi'/\partial A, \partial\psi/\partial B, \partial\psi'/\partial B\right)$

$$\frac{d\mathbf{Y}}{dx} = \begin{pmatrix} y_1' \\ y_2' \\ y_3' \\ y_4' \\ y_5' \\ y_6' \end{pmatrix} = \begin{pmatrix} y_2 \\ -y_2 g_2(x) + g_1(x) y_1 \\ y_4 \\ -y_4 g_2(x) + g_1(x) y_3 \\ y_6 \\ -y_6 g_2(x) + g_1(x) y_5 \end{pmatrix}, \tag{14}$$

we shoot with a boundary condition at $x = x_s \pm \delta$

$$\begin{pmatrix} y_1 \\ y_2 \\ y_3 \\ y_4 \\ y_5 \\ y_6 \end{pmatrix} = \begin{pmatrix} A|x|^{h+1} \pm B|x|^{-h} \\ A(h+1)|x|^h \pm Bh|x|^{-h-1} \\ |x|^{h+1} \\ (h+1)|x|^h \\ \pm|x|^{-h} \\ \pm h|x|^{-h-1} \end{pmatrix}. \tag{15}$$

One changes the unknown constants A and B until

$$\begin{pmatrix} A^{(l+1)} - A^{(l)} \\ B^{(l+1)} - B^{(l)} \end{pmatrix} = \begin{pmatrix} \partial y_1/\partial A & \partial y_1/\partial B \\ \partial y_2/\partial A & \partial y_2/\partial B \end{pmatrix}^{-1} \begin{pmatrix} y_1 - y_1(x = 0 \text{ or } x = x_b) \\ y_2 - y_2(x = 0 \text{ or } x = x_b) \end{pmatrix}, \tag{16}$$

converges at $x = 0$ and $x = x_b$. The value of Δ' is calculated by

$$\Delta' \equiv \frac{A_{III}}{B_{III}} - \frac{A_I}{B_I}. \tag{17}$$

Since we have two unknowns A and B at $x = x_s \pm \delta$, we need additional boundary conditions at $x = 0$ and $x = x_b$ for ψ'. However, the value of Δ' is independent of these additional boundary conditions, since only the ratio A/B in each region I and III is required to obtain Δ'.

Figure 2(a) shows the resultant eigenfunction of an $m/n = 2/1$ mode with $\beta = 7\%$ (h=-0.076) which has singular behavior in the vicinity of the mode rational surface. Here, $x_s = 1$ and $x_b = 2$ were taken. Figure 2(b) expands the singular behavior in the vicinity of x_s; the analytical solutions (dashed line) given by Eqs. (12) and (13) are successfully matched to the numerical solutions (solid line). Figure 2(c) shows the value of Δ' versus β with the layer width set to $\delta = 10^{-7}$. The effect of the finite pressure term decreases the Δ' value, and thus stabilizes the tearing mode, even in a cylindrical tokamak. Note that $D_s \geq 0$ ($h \leq 0$) in a cylinder while $D_s \leq 0$ ($h \geq 0$) for a $q > 1$ surface in a toroidal geometry.[14]

In a $\beta \to 0$ limit, the Δ' value reduces to the zero-pressure case $\Delta' = 1.54$ (see Fig. 1(b)). In this $\beta \to 0$ limit (but with pressure term), the second terms in Eqs. (12) and (13) become constants and reduce to the form of Eq. (8). In Fig. 2(c), the Δ' value in a relatively high β regime ($\beta \geq 7\%$) is calculated correctly. (See Table I for the estimated scale length δ as function of β). Note that the value of Δ' approaches -2 as D_s approaches $1/4$, where the large and the small solutions become comparable. This feature can be predicted analytically from Eq. (17); $A_{III}/B_{III} - A_I/B_I = -1-1 = -2$. These results guarantee that the algorithm is mathematically appropriate.

When $\delta \leq 10^{-8}$, the numerical method becomes troublesome. The limit of the numerical method depends on the ratio of the coefficients $\partial_A y_{1,2}$ and $\partial_B y_{1,2}$ in Eq. (16). For extremely small layer width δ, numerical truncations in calculating the right side of Eq. (16) obscure the mathematical separation between the large and the small solutions.

In a $\beta \to 0$ limit, the characteristic layer scale width for pressure effect $\delta \sim e^{1/h}$ becomes literally infinitesimal (for example, $\delta \sim 10^{-44}$ for $\beta = 1\%$ and $\delta \sim 10^{-6}$ for $\beta = 7\%$, see Table I). However, needless to say, at the same time, the pressure effect becomes negligible. Furthermore, in the range $0\% \leq \beta \leq 7\%$, one can conjecture that Δ' takes on values that smoothly match with $\Delta' = 1.54$ at $\beta = 0$, and the curve of Fig.2(c) in the $\beta \geq 7\%$ regime. Physically, a layer must have a finite width: a layer width δ smaller than the ion Larmor radius (on the order of 10^{-5} even in a plasma of a temperature as low as $100eV$) is only a metaphysical consideration. In short, we see that the shooting method presented here

extracts the finite pressure effects on Δ', within a reasonable parametric regime for tokamak plasmas. Finite pressure effects in toroidal geometry are discussed in the next section.

V. EIGENMODE IN A TOROIDAL GEOMETRY

In a toroidal equilibrium, straight magnetic field lines[21] are represented by

$$B = I(\rho)\nabla\zeta + \nabla\zeta \times \nabla\psi_{eq}(\rho) = \nabla\psi_{eq}(\rho) \times \nabla\left[q(\rho)\theta - \zeta\right], \tag{18}$$

where ζ is the toroidal angle and ρ is the equilibrium magnetic surface label. With a relation $\partial\psi_{eq}/\partial\rho = I\rho/q$, the flux surface averaged exterior equation in toroidal geometry[12] reduces to (small aspect ratio $\epsilon \ll 1$ and $I = const$ assumed for simplicity)

$$\frac{1}{x}\frac{\partial}{\partial x}x\left\langle g^{\rho\rho}\right\rangle\frac{\partial\psi}{\partial x} - \frac{m^2}{x^2}\left\langle g^{\theta\theta}\right\rangle\psi - \frac{mq}{x(m-nq)}\frac{dj}{dx}\psi - \beta\frac{n^2q^2}{x^2(m-nq)^2}\frac{dp}{dx}\frac{d\left\langle R^2\right\rangle}{dx}\psi = 0 \tag{19}$$

where θ is the poloidal angle, $j(x)$ stands for the toroidal current, and $R = R(\rho,\theta)$ stands for the major radius. Here, $\langle\rangle$ stands for a flux surface average. The magnetic well[22] is approximated by $(-x)(d\left\langle R^2\right\rangle/dx)$; as stated in Ref. 12, a more careful derivation of the pressure term yields the "E+F+H" terms of Glasser, Greene, and Johnson.[14] Note that in a cylindrical plasma with a monotonically decreasing current, $d\left\langle R^2\right\rangle/dx \geq 0$, while $d\left\langle R^2\right\rangle/dx \leq 0$ can occur in a torus since a good curvature region (a magnetic well) exists in a tokamak for $q > 1$.[23]

From a mathematical viewpoint, this second order ordinary differential equation gives system of first order equations that are similar to the cylindrical ones, except for the radially dependent functions $\left\langle g^{\rho\rho}\right\rangle$, $\left\langle g^{\theta\theta}\right\rangle$ (metric elements), and $\left\langle R^2\right\rangle$. The toroidicity effects are included in these latter functions. In this study, radial profiles of the flux surface averaged metric elements are obtained from an equilibrium code RSTEQ.[24] Figure 3(a) exhibits the grids of the straight field line, PEST[21] coordinate system — both the equilibrium flux contours and the θ contours at $\beta = 10\%$. In Fig. 3(a), the abscissa $X = (R-1)/\epsilon$ and the ordinate Z are horizontal and vertical dimensionless minor radius coordinates, respectively. In Fig. 3(a), the area of each grids represents the volume element $\nabla\rho \times \nabla\theta \cdot \nabla\zeta = R^{-2}(\rho,\theta)$.

Note that the equation reduces to the cylindrical version of the Newcomb equation[10] (see Appendix A) in the $\langle g^{\rho\rho} \rangle = \langle g^{\theta\theta} \rangle = 1$ limit.

The dashed line in Fig. 3(b) is the eigenmode profile in a toroidal geometry with $\beta = 10\%$ while the solid line is the profile in the cylindrical limit (In Fig. 3(b), β has been taken to be zero in Eqs. (3) and (19) to bring out the Shafranov shift, geometry effects). The safety factor was taken to be $q(x) = 1 + x^2$, so that the $m/n = 2/1$ mode rational surface is located at $x_s = 1.0$ (the plasma boundary located at $x_b = 2.0$). The dashed line (S — Shafranov shift) in Fig. 4(a) shows the value of Δ' as function of β [see Table II for the corresponding Shafranov shift Δ_s; a magnetic axis shift measured in (X, Z) coordinate system]. The distortion of the flux surfaces (Shafranov shift effects) from the first and the second term of Eq. (19) significantly contribute to the decrease of Δ' with β.

The curvature effect[14] is now investigated quantitatively by including the $\beta \neq 0$ curvature term in Eq. (19) . As a reminder, in toroidal geometry the D_s value of Eq.(13) is replaced by[14]

$$D_s \equiv \beta \left(\frac{-q^2}{q'^2 x^2} \right) \left(\frac{dp}{dx} \right) \left(\frac{1}{\langle g^{\rho\rho} \rangle} \frac{d\langle R^2 \rangle}{dx} \right) |_{x=x_s} \simeq \beta \left(\frac{-2q^2}{q'^2 x} \right) \left(\frac{dp}{dx} \right) \left(1 - q^2 \right) |_{x=x_s}, \tag{20}$$

The last relation is given in the limit of large aspect ratio.[23] (The first form of Eq. (20) is employed for computation). Thus, the D_s value in a toroidal system can be negative (h can be positive) when q is above unity. If h is positive, the asymptotic solution given by Eqs. (12) and (13) gives rise to a $1/\mathcal{X}^h$-like singularity ($|\psi| \to \infty$ at $\mathcal{X} \to 0$). In contrast to the $h \leq 0$ case discussed in Sec.IV, the numerical truncation in Eq. (16) will be severe in higher β cases rather than for lower β cases because of the change in the sign of D_s and thus the power h. Figure 4(b) shows an eigenfunction of an $m/n = 2/1$ mode in a torus with $\beta = 7\%$ which has a positive spike in the vicinity of the mode rational surface. This is expected analytically from Eqs. (12) and (13). Figure 4(c) shows the detail of the singular behavior in the vicinity of x_s; the analytical solutions (solid line), Eqs. (12) and (13), are successfully matched to the numerical solutions (dashed line).

The dot-dashed line in Fig. 4(a) shows the value of Δ' as a function of β in the presence

of the pressure term (C — curvature effect) but without toroidal shape effects (the metric elements are set to their cylindrical limits). The solid line in Fig. 4(a) shows the value of Δ' in the presence of both of the effects. As one can see from the difference of the three lines in Fig. 4(a), toroidal geometry effects (S) stabilize the tearing mode significantly even in a low β regime before the curvature effect (C) comes into play, for the typical tokamak q-profile and a pressure profile we have employed (see Fig. 5). More generally, the curvature effect is expected to be modest, unless one enters an extremely high β regime, or extremely low shear region where the $1/q'^2$ in D_s becomes influential. The line (C) in Fig. 4(a) supports this latter fact numerically. Note that the curvature effect is rather a localized layer property, while the Shafranov shift is a global effect obtained via the metric elements.

VI. DOUBLE TEARING MODE

The double tearing mode is considered to be a cause of off axis sawteeth in reversed shear discharges in TFTR,[16] which have a nonmonotonic q-profile. In the case of a double tearing mode, four parameters are needed from the exterior solution. These are defined by[15]

$$\begin{pmatrix} \Delta'_{11} & \Delta'_{21} \\ \Delta'_{12} & \Delta'_{22} \end{pmatrix} = \begin{pmatrix} \left[\psi_1'\left(x_{s1}+\delta\right)-\psi_1'\left(x_{s1}-\delta\right)\right]/\psi_1\left(x_{s1}\right) & -\psi_1'\left(x_{s2}-\delta\right)/\psi_1\left(x_{s1}\right) \\ \psi_2'\left(x_{s1}+\delta\right)/\psi_2\left(x_{s2}\right) & \left[\psi_2'\left(x_{s2}+\delta\right)-\psi_2'\left(x_{s2}-\delta\right)\right]/\psi_2\left(x_{s2}\right) \end{pmatrix}$$

where x_{s1} and x_{s2} correspond to the two mode rational surfaces, and ψ_1 and ψ_2 are the two eigenmode profiles of double tearing modes. The dispersion relation can be written as

$$\left[\Delta'_{11}\left(\gamma\right)-\Delta'_{11}\right]\left[\Delta'_{11}\left(\gamma\right)-\Delta'_{11}\right]-\Delta'_{12}\Delta'_{21}=0. \tag{21}$$

The roots for γ will give the growth rate of the modes.[15] Here, $\Delta'\left(\gamma\right)=\delta\pi\gamma S$, and a layer width is given by $\delta=\left(x_b/nx_s\right)^{1/3}S^{-1/3}$. ($S$ is the Lundquist number. The inner layer properties enter through S which represents the resistivity). An important feature of the double tearing mode is the contribution from the off diagonal elements Δ'_{21} and Δ'_{12} in addition to Δ'_{11} and/or Δ'_{22}. Figure 6(a) shows the nonmonotonic q-profile used in this study:

$$q(x) = q_0 + ax^3 + bx^2 \tag{22}$$

which satisfies $q'(0) = 0$ and $q(0) = q_0$. The profile is similar to that shown in Fig. 5(b) of Ref. 16. Here, fixed values $q_0 = 2.3$ and $x_{s1} = 0.5$ are taken and x_{s2} is varied. Figure 6(b) shows the eigenmode profiles of ψ_1 and ψ_2 obtained in a toroidal geometry with $\beta = 0.12\%$ and $\epsilon = 0.25$. In Fig. 6(b), the dashed line represents the mode rational surfaces x_{s1} and x_{s2}. Figure 6(c) shows the values of Δ' as a function of a distance $x_{s1} - x_{s2}$. Values of Δ' decrease as the distance $x_{s1} - x_{s2}$ increases, except for Δ'_{11}.

This analysis is compared with a numerical simulation from the FAR[17] initial value instability code. The q-profile of Fig. 6(a) has been taken for the equilibrium. The linear growth of an $m/n = 2/1$ mode has been calculated. The dashed line in Fig. 6(d) is the growth rate obtained from the numerical simulation while the solid lines are obtained analytically from Eq. (21). While, as inferred in Ref. 25, the growth rate from Δ' (denoted as $\gamma_{\Delta'}$) decreases as the distance $x_{s1} - x_{s2}$ increases, the growth rate from the simulation (denoted as γ_{FAR}) tend to increase with the distance (this is also true in a cylinder). This feature suggests that the double tearing mode is not merely driven by the current gradient free energy. This discrepancy will be prominent in a higher β equilibrium. Note that, for example $\beta = 2\%$ gives a large Shafranov shift (30% of minor radius for a nonmonotonic q-profile). For comparison, $\gamma_{\Delta'}$ and γ_{FAR} matches well in monotonic q-profiles.

Figure 6(e) shows the radial profile of the eigenfunction $\psi_{2/1}$ obtained from the simulation. This eigenfunction can be regarded as a combination of ψ_1 and ψ_2 in Fig. 6(b). Figures 6(f) and 6(g) show Poincaré plots of field line trajectories in a poloidal cross section; here, the abscissa and ordinate correspond to the major radius and the vertical coordinate, respectively. The trajectories form two chains of $m/n = 2/1$ magnetic islands. Note that the two islands are different in phase by $\pi/2$. For example, the O-point (X-point) of the inner island is located on the same equi-θ line as the X-point (O-point) of the outer island. This is because the helical component of the perturbed magnetic field on the inner surface is in the opposite direction compared to the outer surface, while the parity of the radial

magnetic field perturbation remains the same for both.

The bad (good) curvature side is located to the right (left) in Fig. 6(f). The good (bad) curvature side is located to the left (right) in Fig. 6(g). As one can see, the core region is close to the wall on the bad curvature side of Fig. 6(g). Further simulation studies in the nonlinear stage (off-axis crash phase) together with the ballooning effects and anisotropic pressure effects are currently being studied. However, this is not consistent with the rest of the work in this paper which focuses on the linear phase of the tearing mode, and will be presented as another work.

VII. SUMMARY AND DISCUSSION

In this paper, we have reviewed tearing mode theory and computations in a cylinder and extended the studies to axisymmetric toroidal geometries. A new numerical algorithm that shoots out from the singular surface rather than in toward the singular layer was developed and employed. Numerical results obtained from the shooting code for cylindrical cases matched results obtained previously by Furth et al..[9]

The effect of finite pressure on tearing modes has been discussed. For the first time, the Δ' value as a function of D_s has been reported. It has been shown that, with the new algorithm we employed (shooting away from the mode rational surface rather than into it), shooting methods resolve the singularities[9] due to the finite pressure effect. The method guarantees separation of the large and the small solutions in the vicinity of a resonant surface. It has been demonstrated that the method is convergent for a relatively high β regime ($\beta \geq 7\%$) for cylinders and low β regime ($\beta \lesssim 20\%$) for toroidal geometries. It has been shown that the finite pressure effects stabilize the constant-ψ tearing mode in a high-β ($\beta \geq 7\%$) cylindrical geometry.

In toroidal geometries, it is suggested that the distortion of the flux surfaces by large Shafranov shifts (a macroscopic effect) stabilizes the tearing mode. The magnetic well effect[13] was investigated quantitatively as well. By comparing the change in Δ' as a function

of β, it has been shown that the distortion of the flux surface (or Shafranov shift) stabilizes the tearing mode significantly even in a low β regime (near the β limit) before the magnetic well effect comes into play. Thus we believe that, for practical purposes in estimating Δ' in the linear stage, the pressure term can be neglected unless one enters an extremely high β regime, or an extremely low shear region. Inclusion of the pressure gradient term merely complicates the prediction of tearing mode stability.

A double tearing mode has been studied as an example of a coupled-mode instability, by calculating the off-diagonal elements of Δ' matrix. The analytical growth rate obtained from Δ' is compared with the FAR code simulation.[17] The results suggest that additional effects other than the current gradient contribution determines the linear growth rate of the instability.

The analysis of mode coupling of incommensurate helicity perturbations is beyond the scope of this paper and will be a subject for future work.

ACKNOWLEDGEMENTS

One of the authors (YN) is grateful to Drs. C. Ren and F. L. Waelbroeck for their valuable suggestions. YN also thanks Drs. V. E. Lynch and J-N. G. Leboeuf for a kind assistance for the usage of the equilibrium code RSTEQ. This research was supported by United States Department of Energy Grant No. DE-FG02-86ER53218.

Appendix A: REVIEW OF WESSON'S ANALYSIS AND COMPUTATION

In this section, the results of Ref. 10 will be reviewed. In the large aspect ratio limit, the Newcomb equation Eq.(4) reduces to

$$\psi'' + \frac{1}{x}\psi' - g(x)\psi = 0. \tag{A1}$$

where

$$g(x) = \frac{m^2}{x^2} + \frac{mq}{x(m-nq)}\frac{dj}{dx} + 2\beta\frac{n^2q^2}{x(m-nq)^2}\frac{dp}{dx}. \tag{A2}$$

Wesson[10] used current profiles in the form of $j(x) = (1-x^2)$ and correspondingly $b(x) = x/2 - x^3/4$ and $q(x) = 4\epsilon/(2-x^2)$. Here $\epsilon = (2-x_s^2)\left(q_{m/n}/4\right)$ stands for the inverse aspect ratio. The numerical algorithm applied for Eq. (A1) is the same as in Sec.III. The value of Δ' is calculated by $\Delta' = A_{III} - A_I$ as before. Figure 7(a) shows the eigenmode profile for an $m/n = 2/1$ mode with mode rational surface located at $x_s = 0.5$. Figure 7(b) shows the value of Δ' as a function of mode rational surfaces x_s. The results match with Fig.6.7.1 of Ref. 10.

REFERENCES

1. P. H. Diamond, R. D. Hazeltine, Z. G. An, B. A. Carreras, and H. R. Hicks, Phys. Fluids **27**, 1449 (1984) ; S. Tsuji, Y. Nagayama, K. Miyamoto, K. Kawahata, N. Noda and S. Tanahashi, Nucl. Fusion **25**, 305 (1985).

2. J. D. Callen, B. V. Waddell, B. Carreras, M. Azumi, P. J. Catto, H. R. Hicks, J. A. Holmes, D. K. Lee, S. J. Lynch, J. Smith, M. Soler, K. T. Tsang and J. C. Whitson, in *Plasma Physics and Controlled Nuclear Fusion Research, 1978*, Proceedings of the 7th International Conference, Innsbruck, (International Atomic Energy Agency, Vienna,1979) Vol. 1, p.415.

3. Y. Nishimura and M. Azumi, Phys. Plasmas **4**, 2365 (1997).

4. H. P. Furth, J. Killeen, and M. N. Rosenbluth, Phys. Fluids **6**, 459 (1963).

5. C. Ren, J. D. Callen, T. A. Gianakon, C. C. Hegna, Z. Chang, E. D. Fredrickson, K. M. McGuire, G. Taylor, and M. C. Zarnstorff, Phys. Plasmas **5**, 450 (1998).

6. Z. Chang, J. D. Callen, E. D. Fredrickson, R. V. Budny, C. C. Hegna, K. M. McGuire, M. C. Zarnstorff, and the TFTR Group, Phys. Rev. Lett. **74**, 4663 (1995).

7. A. Pletzer, A. Bondeson, and R. L. Dewar, J. Comp. Phys. **115**, 530 (1994).

8. K. Hoshino, M. Mori, T. Yamamoto, H. Tamai, T. Shoji, Y. Miura, H. Aikawa, S. Kasai, T. Kawakami, H. Kawashima, M. Maeno, T. Matsuda, K. Oasa, K. Odajima, H. Ogawa, T. Ogawa, T. Seike, T. Shiina, K. Uehara, T. Yamauchi, N. Suzuki, and H. Maeda, Phys. Rev. Lett. **69**, 2208 (1992); G. Kurita, T. Tsuda, M. Azumi, T. Takizuka, and T. Takeda, Nucl. Fusion **34**, 1497 (1994); C. C. Hegna and J. D. Callen, Phys. Plasmas **4**, 2940 (1997).

9. H. P. Furth, P. H. Rutherford, and H. Selberg, Phys. Fluids **16**, 1054 (1973).

10. J. Wesson, *Tokamaks*, (Cambridge Press, Cambridge, 1987), p. 150.

11. J. L. Johnson, J. M. Greene, and B. Coppi, Phys. Fluids **6**, 1169 (1963); R. D. Hazeltine and J. D. Meiss, *Plasma Confinement*, (Addison Wisley, New York, 1992), p. 281.

12. C. C. Hegna and J. D. Callen, Phys. Plasmas **1**, 2308 (1994).

13. C. Mercier, Nucl. Fusion **1**, 47 (1960).

14. A. H. Glasser, J. M. Greene, and J. L. Johnson, Phys. Fluids **19**, 567 (1976).

15. R. L. Dewar and M. Persson, Phys. Fluids B **5**, 4273 (1993).

16. Z. Chang, W. Park, E. D. Fredrickson, S. H. Batha, M. G. Bell, R. Bell, R. V. Budny, C. E. Bush, A. Janos, F. M. Levinton, K. M. McGuire, H. Park, S. A. Sabbagh, G. L. Schmidt, S. D. Scott, E. J. Synakowski, H. Takahashi, G. Taylor, and M. C. Zarnstorff, Phys. Rev. Lett. **77**, 3553 (1996).

17. L. A. Charlton, J. A. Holmes, H. R. Hicks, V. E. Lynch, and B. A. Carreras, J. Comput. Phys. **63**, 107 (1986); Y. Nishimura, J. D. Callen, and C. C. Hegna, UW-CPTC-13, to be submitted to Phys. Plasmas.

18. G. Schmidt, *Physics of High Temperature Plasmas*, (Academic Press, New York, 1979), p. 146.

19. W. A. Newcomb, Ann. Phys. **10**, 232 (1958).

20. M. Abramowitz and I. A. Stegun, *Handbook of Mathematical Functions*, (Dover, New York, 1970), p. 896.

21. R. C. Grimm, J. M. Greene, and J. L. Johnson, Meth. Comput. Phys. **9**, 253 (1976).

22. J. M. Greene, Comments Plasma Phys. Controlled Fusion **17**, 389 (1997).

23. V. D. Shafranov and E. I. Yurchenko, Soviet Phys. JETP **26**, 682 (1968).

24. V. E. Lynch, B. A. Carreras, H. R. Hicks, J. A. Holmes, and L. Garcia, Comput. Phys. Commun. **24**, 465 (1981).

25. Q. Yu, Phys. Plasmas **3**, 2898 (1996).

TABLES

Table I. The relation between β, h, and δ. Here, $D_s = \beta$ with a peaked profile.

β (%)	h	Layer width δ
1	-0.010	3.7×10^{-44}
5	-0.053	6.3×10^{-9}
7	-0.076	1.9×10^{-6}
10	-0.11	1.1×10^{-4}
20	-0.27	2.1×10^{-2}

Table II. The relation between β and Shafranov shift Δ_S in the equilibrium with $q(x) = 1 + x^2$.

β (%)	Δ_s
1	0.14
2	0.21
3	0.27
5	0.36
10	0.48
20	0.60

FIGURES

FIG. 1. (a) The eigenmode profile for an $m/n = 2/1$ mode. The position of the mode rational surface x_s, indicated by dashed lines, is varied. These results correspond to Fig. 2 of Ref. 9. (b) Values of Δ' as a function of x_s, which corresponds to the $m = 2, x_b = 2$ case of Fig. 1 of Ref. 9.

FIG. 2. (a) The eigenmode profile for an $m/n = 2/1$ mode. (b) Expansion of the eigenfunction behavior in the vicinity of x_s. Both analytical solutions (solid line) and the numerical solutions (dashed line) are shown. (c) Δ' versus β in the high β ($\beta \geq 7\%$) regime. The dashed line signifies regions where layer widths wider than physical ones ($\delta \sim e^{1/h}$) are imposed.

FIG. 3. (a) The equilibrium flux surfaces and θ contour lines in a toroidal geometry with $\beta = 10\%$ which show geometrical distortions. (b) The eigenmode profile of $\psi_{2/1}$. The solid line is for a toroidal geometry with $\beta = 10\%$ and the dashed line is for a cylindrical limit (the pressure gradient drive term in the eigenmode equation is absent for both lines).

FIG. 4. (a) Δ' as function of β, [S (Shafranov) indicates in the absence of the pressure gradient drive term but with toroidal shape, C (curvature) in the presence of pressure gradient drive term but without toroidal geometrical effects ($\langle g^{\rho\rho} \rangle = \left\langle g^{\theta\theta} \right\rangle = 1$), and S+C both the toroidal effects and pressure-drive effects present]. (b) The eigenmode profile of an $m/n = 2/1$ mode with $\beta = 7\%$. (c) Expanded eigenfunction in the vicinity of x_s. Analytical solutions (solid line) and the numerical solutions (dashed line) are both shown.

FIG. 5. The Grad-Shafranov equilibrium pressure profile employed for Fig. 4(a), (b), and (c).

FIG. 6. (a) A nonmonotonic q-profile. The minimum value located is at $x_{min} = 1$. (b) The eigenmode profiles for ψ_1 and ψ_2. The vertical dashed lines represent the mode rational surfaces x_{s1} and x_{s2}. (c) The values of Δ' as a function of a distance $d = x_{s1} - x_{s2}$. Values of Δ' decrease as the distance $x_{s1} - x_{s2}$ increases. (d) The linear growth rate of the $\psi_{2/1}$ mode as a function of a distance $d = x_{s1} - x_{s2}$ obtained from simulation. (e) The eigenmode profile of the $\psi_{2/1}$ mode obtained from the numerical simulation. (f) Poincaré mappings of magnetic field line trajectories, at a toroidal angle $\zeta = 0$. (g) Poincaré mappings at a toroidal angle $\zeta = \pi$.

FIG. 7. (a) The eigenmode profile for an $m/n = 2/1$ mode. (b) Δ' versus x_s. These results corresponds to Fig. 6.7.1 of Ref. 10.

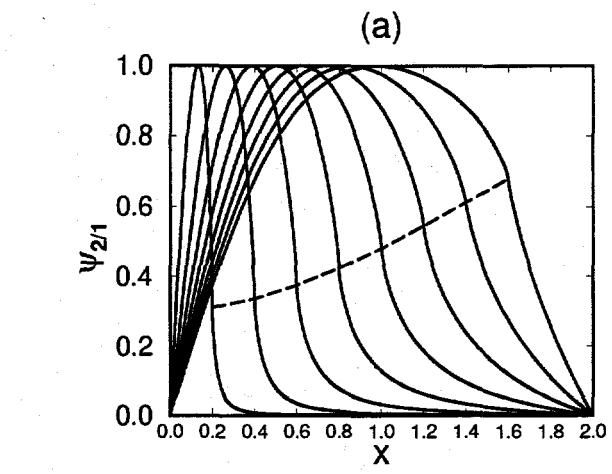

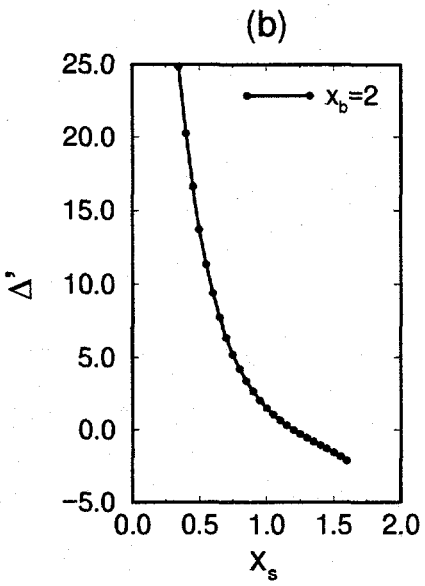

Fig.1 Yasutaro Nishimura

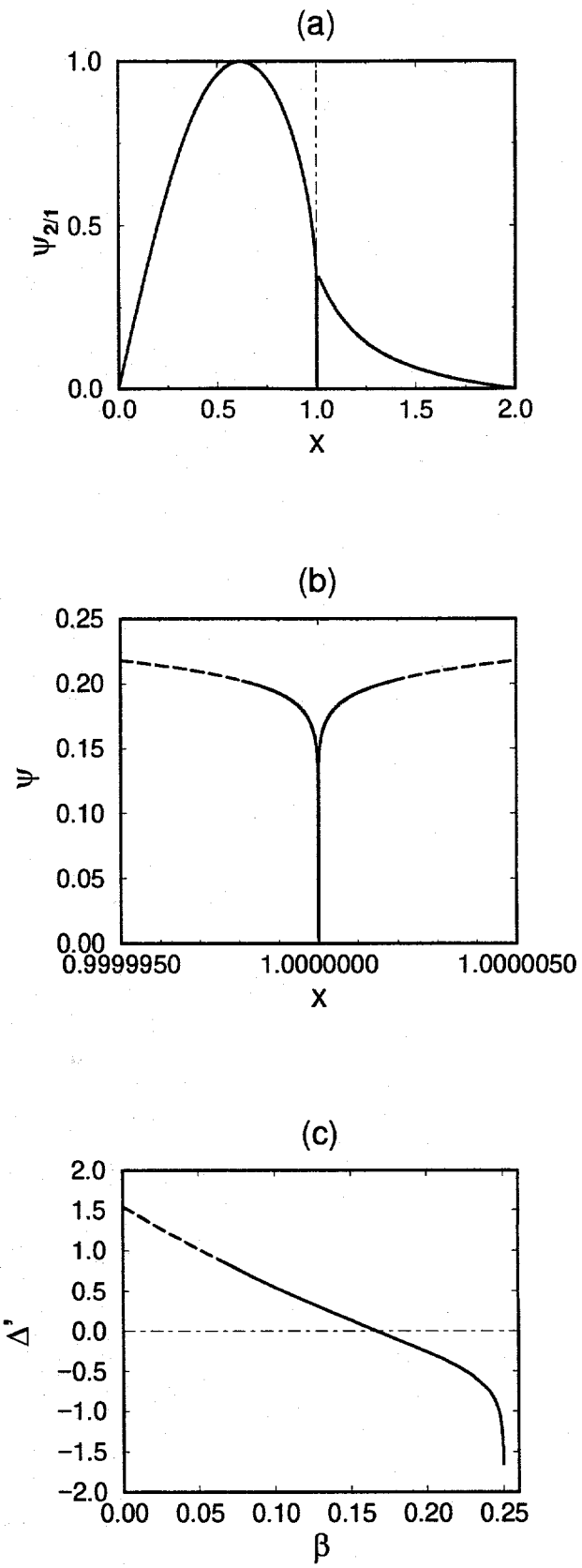

Fig.2 Yasutaro Nishimura

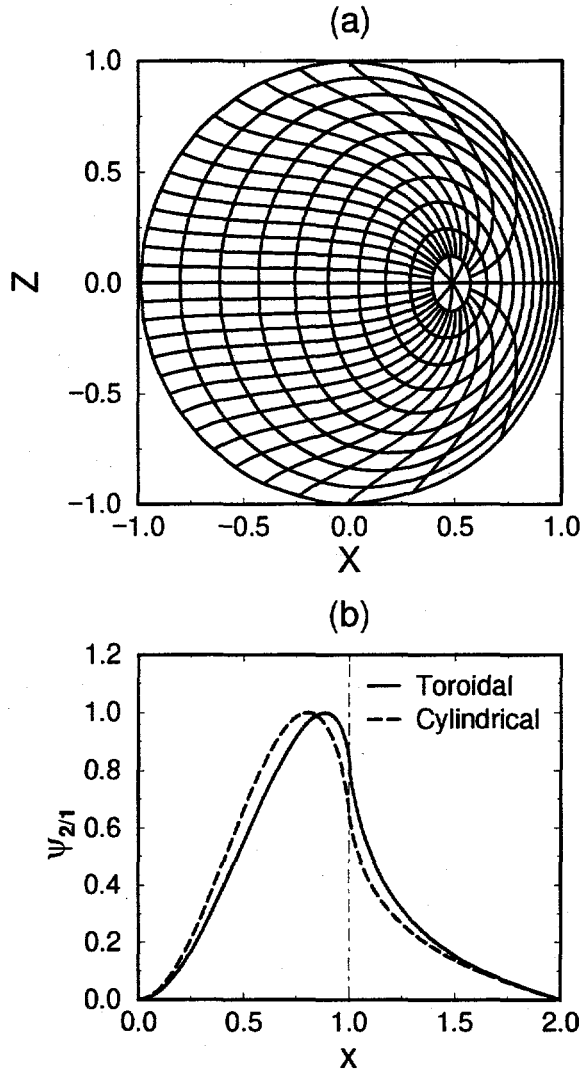

Fig.3 Yasutaro Nishimura

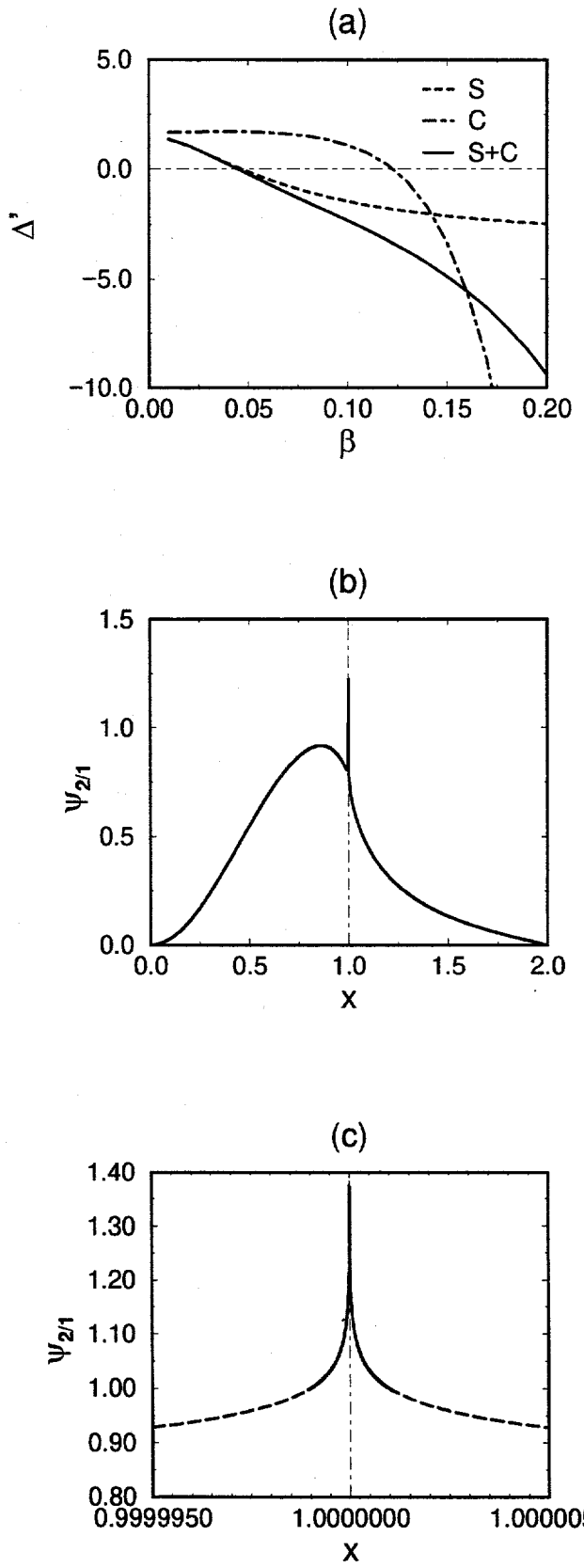

Fig.4 Yasutaro Nishimura

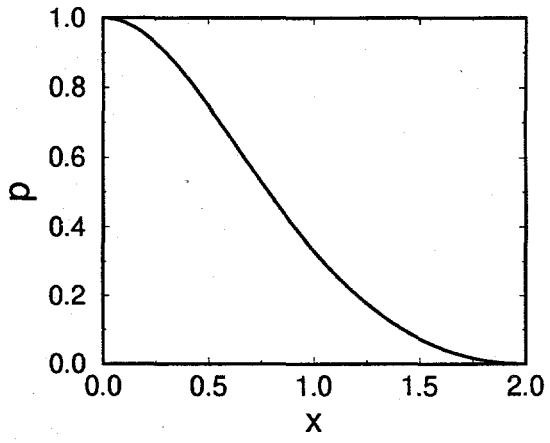

Fig.5 Yasutaro Nishimura

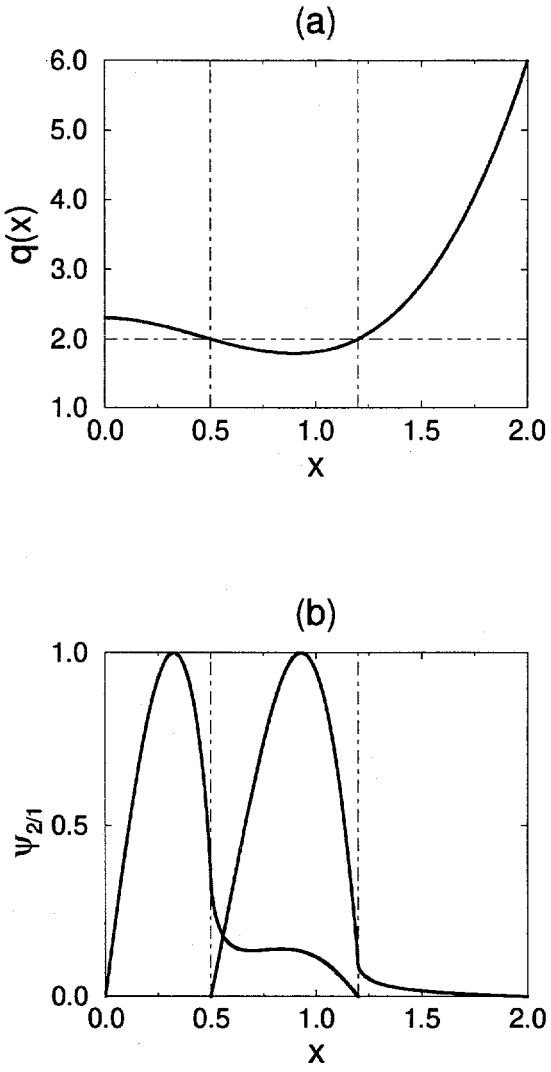

Fig.6 Yasutaro Nishimura

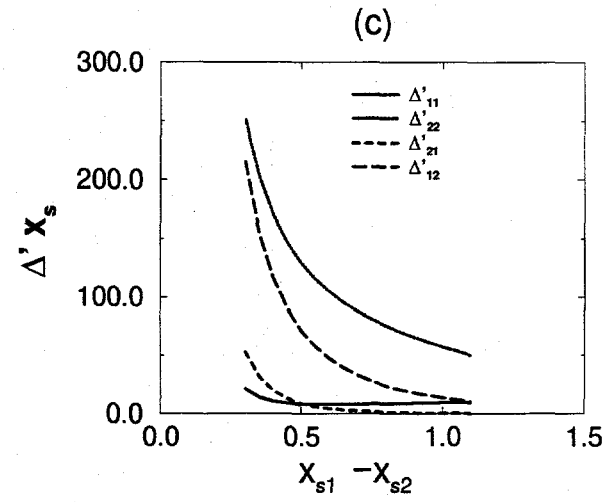

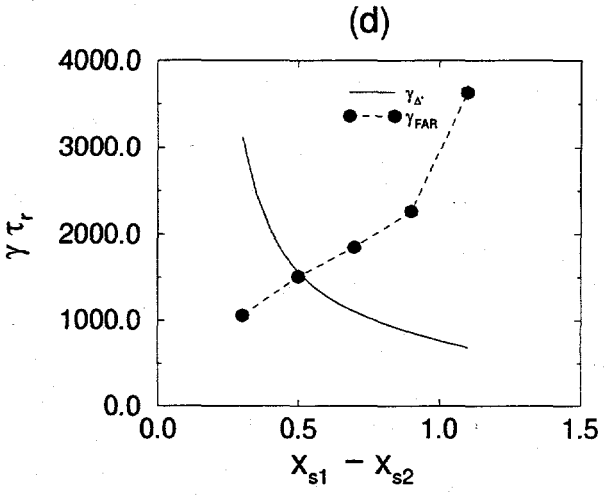

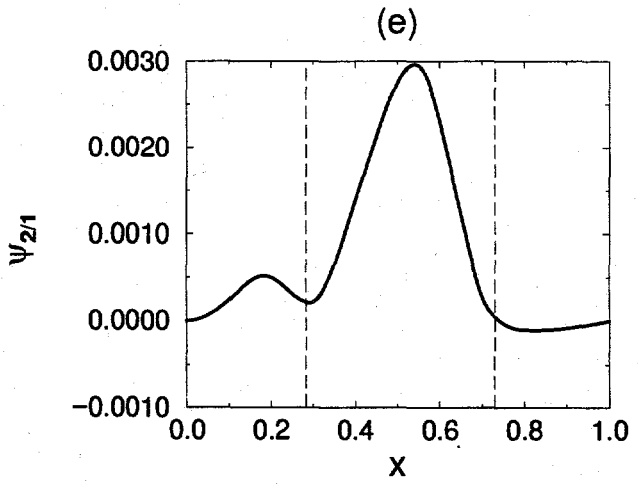

Fig.6 Yasutaro Nishimura

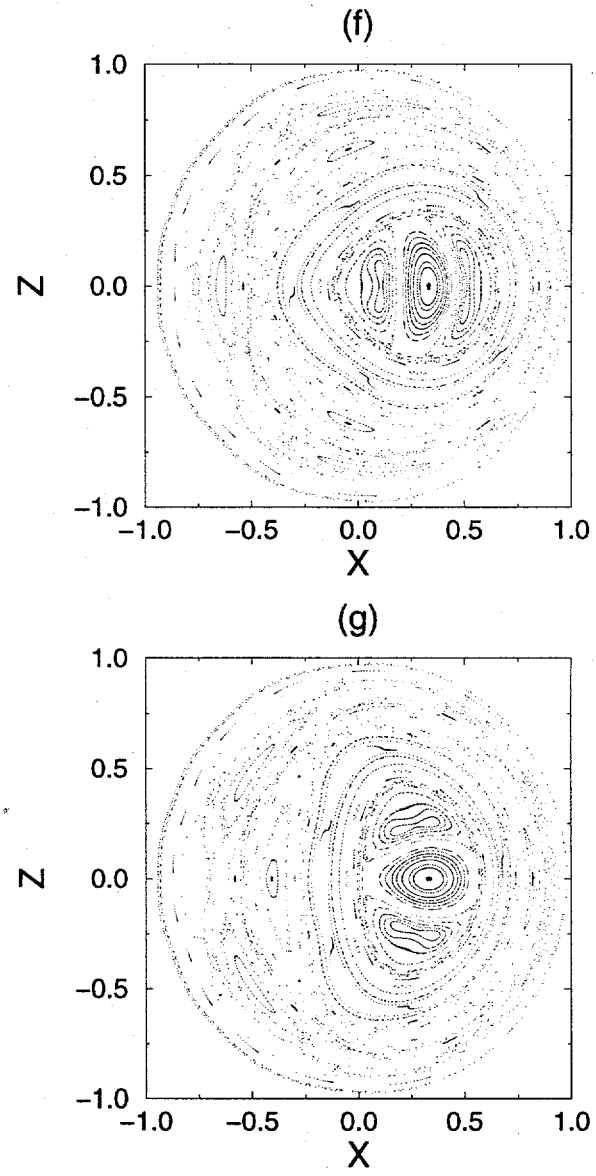

Fig.6 Yasutaro Nishimura

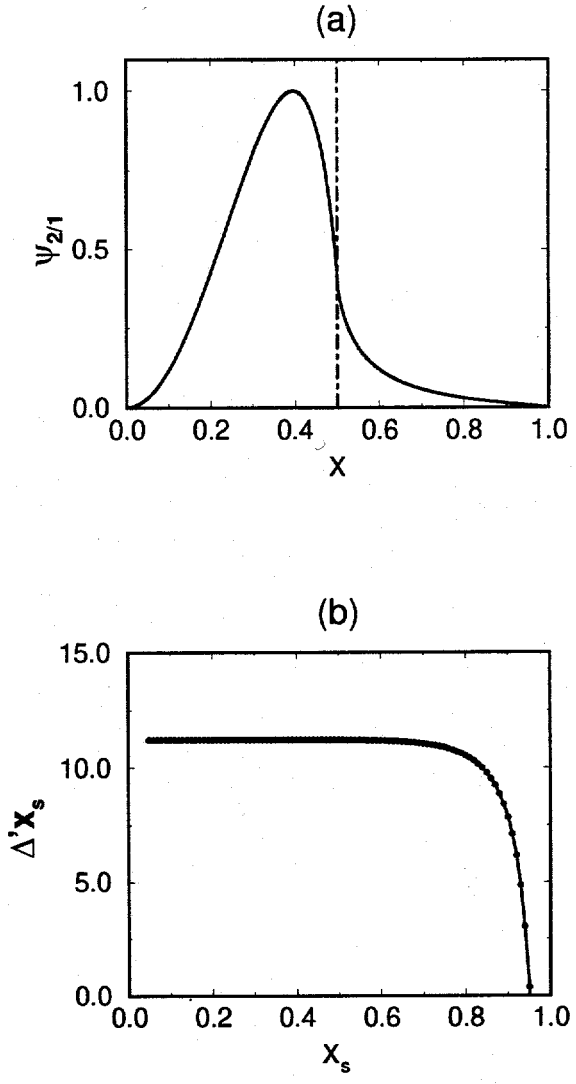

Fig.7 Yasutaro Nishimura